Transverse modulation of an electron beam generated in self-modulated laser wakefield accelerator experiments

C. I. Moore,[1] K. Krushelnick,[2,*] A. Ting,[1] H. R. Burris,[1] R. F. Hubbard,[1] and P. Sprangle[1]
[1]*Plasma Physics Division, Naval Research Laboratory, Washington, DC 20375*
[2]*Laboratory of Plasma Studies, Cornell University, Ithaca, New York 14853*
(Received 9 June 1998; revised manuscript received 17 August 1999)

Low energy electron beams ($E \sim 300$ keV) generated in a self-modulated laser wakefield accelerator experiment were observed to filament and be deflected away from the laser axis forming radial jets in the electron beam profile. At higher energies ($E > 900$ keV), the filamentation and jets were suppressed and smooth electron beams copropagating with the laser were observed. The observed electron beam filamentation likely results from laser beam filamentation in the plasma due to relativistic self-focusing effects. The radial jets of low energy electrons are likely caused by transverse ejection of the electrons due to the radial structure of the wakefield and space charge deflection of electrons as they exit the laser focus.

PACS number(s): 52.40.Nk, 41.75.Lx, 41.75.Fr, 52.35.Qz

Rapid developments in high power laser technology during the past several years have allowed experimental examination of new phenomena resulting from the interaction of ultrahigh intensity light with plasma [1]. Ponderomotive forces associated with high intensity laser pulses can produce larger amplitude plasma waves in the ''wake'' of the laser pulse as it propagates through an underdense plasma and the large electric fields associated with such waves have been proposed as a means of accelerating electrons [2]. There have been several recent experiments which have measured the temporal evolution of plasma waves in the wakefield [3,4], as well as the energy of electrons accelerated by these waves (up to 100 MeV) [5–8].

In the self-modulated laser wakefield acceleration scheme (SM-LWFA) [9], a very high power laser pulse is focused into underdense plasma such that an instability is induced which modulates the laser pulse envelope at the plasma frequency [$\omega_{pe} = (4\pi n_e e^2/m_e)^{1/2}$]. The subsequent resonant interaction with the plasma can produce large amplitude plasma waves in the wake of the pulse which have longitudinal electric fields suitable for accelerating electrons.

In this paper, we discuss recent measurements of accelerated electrons generated during SM-LWFA experiments at the Naval Research Laboratory (NRL). The low energy electron ''beam'' profiles showed structures characteristic of filamentation in the center of the profile and radial jets outside the laser cone angle. High energy electrons showed relatively weaker jets and no filamentation in the center of the profiles. The use of circularly polarized light which may have been expected to axially ''guide'' the electrons through the generation of an axial magnetic field via the inverse Faraday effect was not found to have a significant effect on beam propagation.

The experiment was performed using the Table Top Terawatt (T^3) laser facility at NRL. The laser operates at a wavelength of 1054 nm and a typical power of 2.5 TW ($\tau_{laser} \approx 400$ fsec). The beam was focused using an $f/4$ off-axis parabolic mirror into the front of a jet of helium gas. The helium was completely ionized by the front part of the pulse and the main part of the beam interacted with a plasma having an electron density of $1.4 \times 10^{19}\,\mathrm{cm}^{-3}$ ($n_e \sim 0.01 n_{crit}$). The peak intensity was $6 \times 10^{18}\,\mathrm{W/cm}^2$ when focused in vacuum.

The interaction of the high intensity pulse with the gas jet plasma produced a large number of energetic electrons ($N_e \sim 10^8$) which propagated in the forward direction (along with the laser pulse). This beam of high energy electrons accelerated from the background plasma was highly directional, although it typically had a large energy spread, with many fewer electrons produced at the highest energies. The electron energy spectrum from 500 keV to 4 MeV is shown in Fig. 1. This spectrum was measured using an electromagnet to disperse the electrons in energy and using Kodak direct exposure film (DEF) film as the detector [7]. Higher energy electrons (where the electron fluence was not large enough to expose the film) were measured using a higher sensitivity detector consisting of a plastic scintillator directly coupled to a PMT [7,8].

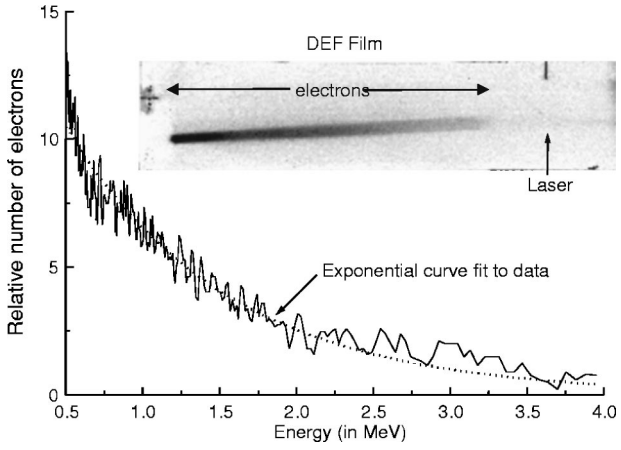

FIG. 1. SM-LWFA accelerated electron energy spectrum from 500 keV to 4 MeV measured using DEF film as the detector. The dark streak on the film is exposure from electrons with a spatial dependence on energy due to an applied magnetic field.

*Present address: Blackett Laboratory, Imperial College, London SW7 2BZ, U.K.

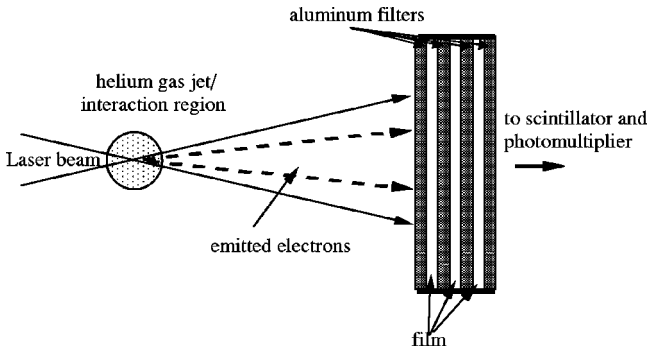

FIG. 2. Electron beam profile measurement experimental setup.

The profile of the electron beam accelerated in the laser plasma interaction was recorded by placing DEF film directly in the path of the electron beam with no intervening magnet (see Fig. 2). Three pieces of film were placed in a ''sandwich'' with two layers of 1 mil (25 μm) aluminum foil before each piece of film and black tape surrounding the entire film pack. In this arrangement each piece of film recorded the profile of subsequently higher energy components of the electron beam. This arrangement was necessary because of large shot-to-shot fluctuations in the emission of high energy electrons which required that different energy components of the electron distribution be observed on a single shot basis. The energy binning was determined by the thickness of aluminum, tape, and film in front of each piece of DEF. For the data shown here (see Fig. 3), we measured energy components of the beam such that $E_A > 300\,\mathrm{keV}$, $E_B > 600\,\mathrm{keV}$, and $E_C > 900\,\mathrm{keV}$. The figures are digitized images of the film with light areas indicating the highest fluence of electrons and darker areas indicating lower electron fluences. The contours are linear steps in relative electron fluence with 6% increments from 0% to 96% of the maximum fluence. Each figure has been adjusted for maximum contrast.

The film pack was placed at a sufficient distance ($d \sim 20\,\mathrm{cm}$) from the interaction region so that the laser beam did not cause breakdown on the exterior of the film pack which might generate hard x rays and expose the film. In addition, a control piece of film was placed perpendicular to the beam profile film and out of the electron beam path to determine if x rays generated in the film pack or elsewhere were sufficient to expose the ''control'' film. No exposure of the control was observed. A plastic scintillator connected to a photomultiplier tube was positioned behind the film pack (Fig. 2) which measured the high energy electrons capable of passing completely through the film pack. The scintillator-photomultiplier sensitivity was much higher than the film's and for a typical shot taken during these experiments, measurement of a highly saturated PMT signal was necessary before adequate exposure of the film could be obtained on a single shot.

Typically, we observed large shot-to-shot fluctuations in the emission of energetic electrons which were uncorrelated with laser pulse energy (except that for low power laser shots, high energy electrons were never observed). The size of the fluctuations was observed to be a few orders of magnitude greater than the noise level. This was somewhat expected since the mechanisms driving the production of the wakefield as well as the trapping and acceleration of background electrons by large amplitude plasma waves during the interaction are plasma instabilities. This implies that small fluctuations in the incident laser energy, beam profile, and focusing characteristics may lead to large changes in the number and energy of accelerated electrons [8].

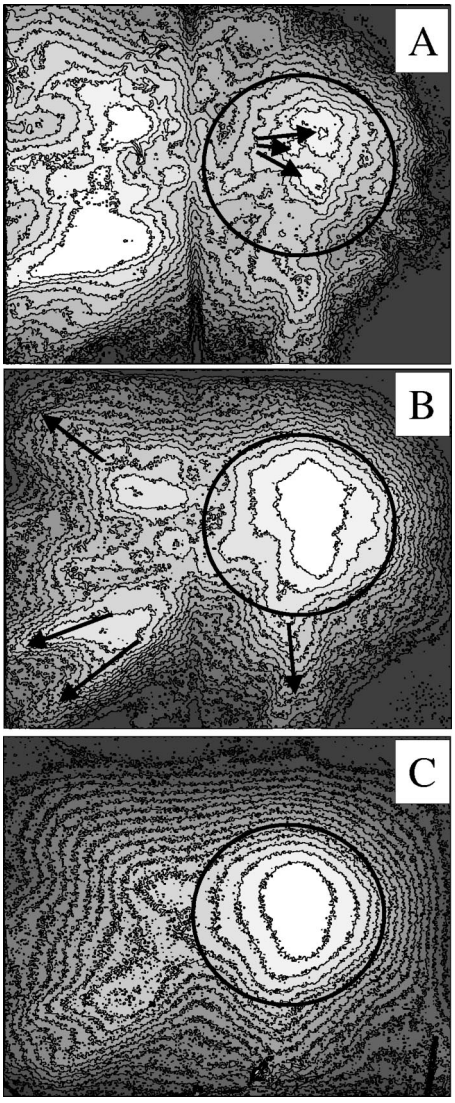

FIG. 3. Electron beam profiles for different energy electrons using circularly polarized light: (a) $E > 300\,\mathrm{keV}$, (b) $E > 600\,\mathrm{keV}$, (c) $E > 900\,\mathrm{keV}$. The diameter and position of the laser beam is indicated by the black circles. The arrows in (a) highlight the electron beamlets indicative of filamentation. The arrows in (b) highlight the direction of the electron ''jets'' radiating outward from the laser cone angle. The contours are linear steps in relative electron fluence with 6% increments from 0% to 96% of the maximum fluence.

The spatial profiles of the accelerated electron beam had two significant characteristics. The first was a large number of electrons outside the laser cone angle (the laser cone angle is represented by the black circle in the three images in Fig. 3), which seemed to radiate outward from the center of the laser cone angle. This is particularly evident in Fig. 3(b), where four of these ''jets'' have been indicated with arrows. The second characteristic observed was small scale structure in the low energy electron distributions [see Fig. 3(a)], which

is characteristic of a filamentation instability. This filamentation is most clearly seen in Fig. 3 by comparing the electrons within the circle in the low energy distribution [Fig. 3(a)], where significant small scale structure is observed (indicated by the arrows), with the electrons within the circle in the high energy distribution [Fig. 3(c)], where only a smooth intensity distribution with a size on the order of the size of the laser beam is observed. Both the jet and filamentation structures were consistently observed on multiple shots, although their locations and intensities were not reproducible. It is also evident in Fig. 3 that both the jet structures and small scale structures were suppressed as the electron energy increased. The suppression of jets is evident by comparing Fig. 3(a) with Fig. 3(c) and noting that more electrons were observed to the left of the laser cone angle than within the laser cone angle in Fig. 3(a), while more electrons were observed within the laser cone angle than outside the laser cone angle in Fig. 3(c). The suppression of the filamentation is evident by noting that the small scale structure visible within the laser cone angle in Fig. 3(a), is completely absent in Fig. 3(c). Scattering of the electrons as they pass through the aluminum and the first layer(s) of film and the resultant blurring may be partially responsible for the lack of filamentation structures at the higher energies. However, blurring from electron scattering (which we estimate to be less than 30° rms [10]) should cause a blurring on the same scale or less than the thickness of material penetrated. For the 900 keV piece of film this thickness was approximately 1 mm, which is much smaller than the transverse structure in the profiles (the pictures shown are approximately 9 cm on a side).

The filamentary structure observed in the electron beam has two possible sources: the laser filamentation instability (LFI) [11] due to nonlinear atomic self-focusing (ASF) [12] and relativistic self-focusing [13] (RSF), or the electromagnetic filamentation (Weibel) instability (EFI) [14–16]. The LFI can cause electron beam filamentation by generating multiple self-focused laser filaments which subsequently drive multiple wakefield filaments and electron beams. The EFI can directly drive electron beam filamentation through the electron beam/plasma instability that develops as a current neutralized electron beam propagates through a relatively dense plasma.

Laser filamentation occurs in a medium when an intensity dependent polarization of atoms or ions [atomic self-focusing (ASF)] and /or an intensity dependent variation in the electron mass due to relativistic effects [relativistic self-focusing (RSF)] causes an intensity dependent variation in the medium's index of refraction. The LFI has a maximum growth rate of [11]

$$\Gamma = (\omega_p^2 a_0^2/8\omega_0)(1+3R/2), \tag{1}$$

with a characteristic filament dimension of $r_\perp = (4c/\omega_p a_0)(1+3R/2)^{-1}$, where a_0 is the normalized vector potential of the laser pulse ($a_0 = eA_0/mc^2$) and R is the ratio of the critical power for RSF to the critical power for ASF. In our experiment, R is negligible near focus ($I \sim 5 \times 10^{18}\,\mathrm{W/cm^2}$) since the helium is completely ionized at approximately $10^{16}\,\mathrm{W/cm^2}$ and there are no atoms or ions left to be polarized. The growth rate for the laser filamentation instability is therefore approximately $10^{13}\,\mathrm{sec}^{-1}$ or an *e*-folding time of 100 fsec. This growth rate is for filaments with a characteristic transverse dimension, $r_\perp$, of approximately 3 μm. A substantial growth rate ($\Gamma > 10^{12}\,\mathrm{sec}^{-1}$) will also be observed for filaments down to a dimension of approximately 2 μm. These rates and dimensions suggest LFI should play an important role in our experiment which is supported by measurements of the laser beam profile.

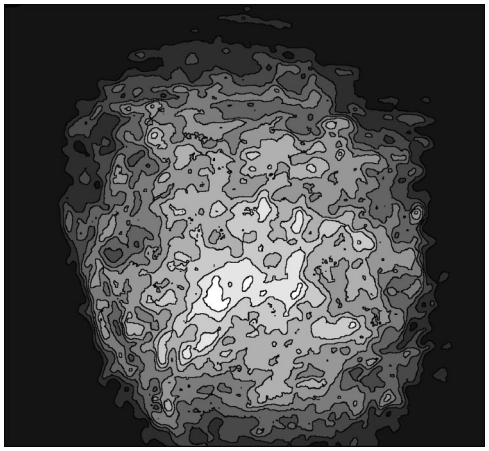

FIG. 4. Profile of laser beam after interaction. This profile exhibits a depth of intensity modulations of nearly 100%, while profiles without interaction are nearly flat top with less than 10% depth of modulation. The contours are linear steps in burn paper exposure at 10% increments from 0% to 90% of the peak exposure.

Laser beam filamentation was always observed in the experiment when the gas jet was fired (a smooth flat top laser profile was observed without the gas jet firing). Figure 4 shows a ''picture'' of the filamented laser beam profile that was taken by placing thermal burn paper over the DEF film pack. The contours are linear steps in burn paper exposure at 10% increments from 0% to 90% of the peak exposure. The observed laser filamentation was not due to ASF effects since measurements of the laser profile with hydrogen in the gas jet showed similar profiles to those obtained using helium in the gas jet. If ASF effects played a substantial role in the observed filamentation, a significant difference would be expected between the hydrogen and helium results since hydrogen is completely ionized at approximately an order of magnitude lower intensity than helium. The electron beam and laser beam profiles shown in Figs. 3 and 4 allow only a qualitative comparison between the electron beam and laser profiles in the focus. This is because diffractive effects dominate the laser propagation from the focus to the image plane (the plane of Figs. 3 and 4) while the electrons travel ballistically with negligible wave properties. Qualitatively, the most striking similarity is the presence of small scale structure in both images which is likely due to the LFI and its resultant mapping on the electron distribution. The most striking difference is the lack of any jets in the laser profile, which will be discussed following a discussion of the second possible source of the observed electron beam filamentation, the electromagnetic filamentation instability (EFI).

The EFI arises when a macroscopically current neutralized low density electron beam propagates through a relatively high density plasma ($n_e \gg n_b$, where n_b is the electron beam density). The electron beam current generated by the wakefield in our experiment (although on the order of a pi-

cosecond in duration [4] and approximately 100 amps) can be effectively neutralized by the plasma since the charge neutralization time, τ_n, is about 100 fsec for a low temperature, high density ($T_e \sim 100$ eV, $n_e \sim 10^{19}$ cm^{-3}) helium plasma ($\tau_n = \eta/4\pi$, where η is the Spitzer resistivity). A neutralized electron beam propagating in a relatively dense plasma is unstable to the EFI when $\gamma_b \omega_{pb}^2 \beta_b^2 / \omega_{cb}^2 > 1$, where the subscript b refers to the electron beam parameters of: γ_b = the relativistic factor, ω_{pb} = the plasma frequency, β_b = the beam velocity normalized to c, and $\omega_{cb} = eB/mc$ (the cyclotron frequency in applied magnetic field B). In this regime, a small scale nonuniformity in current flow will generate a local magnetic field resulting in a pinching of the electron beam or the plasma return current, which further enhances the nonuniformity, which feeds back and creates the instability. The growth rate of the filamentation instability for small scale transverse perturbations of wave number $k_\perp$ such that $c^2 k_\perp^2 \gg \omega_{pe}^2$ is given by [15]

$$\Gamma = \frac{\omega_{pb}\beta_b}{\gamma_b^{1/2}} \left[1 - \frac{\omega_{cb}^2}{\gamma_b \omega_{pb}^2 \beta_b^2} \right]^{1/2}. \tag{2}$$

The maximum electron beam density, n_b, in our experiments was approximately 2×10^{16} cm^{-3}. This density was determined by dividing the measured number of electrons accelerated above 300 keV ($N_b \sim 3 \times 10^8$) by the minimum beam volume, which assumes the electron beam has a length equal to the laser pulse length ($c\tau = 120\ \mu$m) and a radius equal to the laser spot size ($w_0 \approx 6\ \mu$m). The maximum growth rate of the EFI in our experiments was therefore 5×10^{12} sec^{-1} or a minimum e-folding time of 200 fs. This smaller growth rate for the EFI which will be further decreased by the high effective temperature of our electron beam [16] strongly suggests that the EFI is not the dominant source of the filaments observed in the electron beam profile. In addition, we attempted to suppress any EFI induced electron beam filamentation through an applied axial magnetic field. As is apparent in Eq. (2), an applied axial magnetic field of sufficient magnitude (>500 kG for our experimental parameters) can completely suppress the EFI. We attempted to generate this large axial magnetic field through the use of the inverse Faraday effect [17,18]. The inverse Faraday effect is a magneto-optical phenomenon in which the propagation of a circularly polarized laser beam through a nonlinear medium induces a magnetic field along the direction of propagation. For laser-plasma interactions using the parameters of our experiment, theoretical calculations predict the generation of magnetic fields of 1–2 Mgauss [18]. From Eq. (2), a magnetic field of this magnitude should greatly inhibit the growth of the filamentation instability. In our experiments, however, we observed no significant change in the profile of the accelerated electrons using linearly or circularly polarized light. This suggests either the electron beam filamentation was not caused by the EFI or the inverse Faraday effect did not produce the predicted axial magnetic field.

Tzeng *et al.* [19] have performed 2D numerical simulations of a SM-LWFA using parameters very close to those used in our experiment, but with higher laser powers ($P \sim 8$ TW). Their simulations show that lower energy electrons in the SM-LWFA are accelerated at larger angles to the laser axis than the higher energy electrons. In addition, substantial transverse structure was observed in the electron beams after leaving the plasma. This change in ejection angle with energy and the transverse structure were attributed by Tzeng to the focusing and defocusing [20] of the electrons due to the radial structure of the plasma wave [21] and space charge effects as the electrons exit the plasma. The radial wakefield structure causes a change in ejection angle with energy since electrons on axis will experience the strongest acceleration and least radial forces (resulting in higher energy), while electrons off-axis will experience weaker acceleration and stronger radial forces (resulting in lower energy but larger transverse momentum). Space charge effects as the beam exits the plasma were shown to strongly affect the electron trajectories resulting in pronounced transverse structure in the electron beam (see Fig. 4a of Ref. [19]). These effects resulted in electrons ejected at angles up to $\sim 15°$ from the laser axis and electron pulses with centroids off axis. Even though this simulation used a higher laser power and observed a much larger number of accelerated electrons than observed in our experiment ($n_{sim} \sim 10^{11}$ versus $n_{\text{expt}} \sim 10^8$), the transverse distribution of accelerated electrons are very similar. Our experiment observed the strong dependence of ejection angle on energy and radial jets extending to approximately 17° off the laser axis. These jets are likely the three-dimensional manifestation of the space charge induced transverse asymmetries observed in the two-dimensional simulations. The strongest difference between the simulation and our experiment is the three orders of magnitude difference in the number of accelerated electrons. This difference is likely due to the difference in powers used in the experiment and simulation (2.5 TW versus 8 TW). In previous experiments performed at NRL [8], we have seen electrons accelerated in the SM-LWFA with no evidence for wavebreaking. In these previous experiments, a small fraction of electrons were preaccelerated by backward Raman scattering (BRS), trapped in the wakefield, and further accelerated to approximately 100 MeV. The majority of electrons remained oscillatory in the plasma wave and were not accelerated. In the higher power simulation by Tzeng *et al.*, wavebreaking occurs which results in a much larger fraction of accelerated electrons. This larger fraction of accelerated electrons at higher laser powers has also been observed in experiments [6].

Another possible candidate for generating the electron jets is the laser hose instability [22]. The laser hose instability occurs when a laser pulse with a slightly tilted centroid relative to $\vec{k}$ propagates in plasma. This tilted centroid will generate an asymmetric plasma density distribution, which will further enhance the centroid displacement providing the feedback necessary for the instability. The laser hose instability results in a periodic deflection of the laser pulse transverse centroid, which causes the laser pulse to ''snake'' through the plasma. Since the wakefield will follow the laser pulse, this instability will generate a ''kinked'' wakefield, which will accelerate electrons in a straight line for only short distances (resulting in lower energies) and in directions other than the initial laser pulse propagation direction. This would explain the observed electron beam profiles that exhibit relatively stronger jets at the lower electron energies. However, the lack of any associated jets in the laser profile

(Fig. 4, which should also show jets due to deflection from the original laser propagation direction) suggests the laser hose instability is not significant in these experiments. This is further supported by our unsuccessful attempts to observe hosing by imaging the 90° Thomson scattering of the laser (relative to $\vec{k}$) as it passed through the plasma onto a charge-coupled-device camera through a 1054 nm interference filter (bandwidth$\approx$10 nm).

In conclusion, these experiments have measured the effects of the laser filamentation instability, radial wakefields, and space charge effects on the electron beam generated in a SM-LWFA. Low energy electrons from the SM-LWFA were observed to filament within the cone angle of the laser and be radially ejected in jets outside the cone angle of the laser. The observed electron beam filamentation results from a mapping of the laser beam filamentation due to RSF in the plasma into the electron beam profile. The electromagnetic filamentation or Weibel instability is not a likely candidate for the observed filamentation due to a slower growth rate than the LFI and unsuccessful attempts to suppress the EFI through application of an axial magnetic field using the inverse Faraday effect. The electron jets outside the laser cone angle most likely results from a combination of radial ejection of the electrons due to the radial structure in the wakefield plasma wave and space charge forces exerted on the electrons as they exit the plasma. It is less probable that the electron jets were produced by the laser hose instability, since evidence of hosing was not observed in both the transmitted laser profiles and 90° Thomson scattering images. The observation that both the filamentation and jet structures are suppressed for higher energy electrons suggests that these transverse asymmetries are not a problem for high energy laser wakefield accelerators. In fact, the improved directionality of the electron beam with increasing energy shows that a high energy excellent emittance beam can be generated in a laser wakefield accelerator.

This work was supported by the Office of Naval Research and the U.S. Department of Energy.

[1] M. Perry and G. Mourou, Science **264**, 917 (1994).
[2] T. Tajima and J. M. Dawson, Phys. Rev. Lett. **43**, 267 (1979).
[3] J. R. Marquès *et al.*, Phys. Rev. Lett. **76**, 3566 (1996); C. W. Siders *et al.*, *ibid.* **76**, 3570 (1996); S. P. Le Blanc *et al.*, *ibid.* **77**, 5381 (1996).
[4] A. Ting *et al.*, Phys. Rev. Lett. **77**, 5377 (1996).
[5] K. Nakajima *et al.*, Phys. Rev. Lett. **74**, 4428 (1995); C. A. Coverdale *et al.*, *ibid.* **74**, 4659 (1995).
[6] A. Modena, *et al.*, Nature (London) **377**, 606 (1995); R. Wagner *et al.*, Phys. Rev. Lett. **78**, 3125 (1997); D. Gordon *et al.*, *ibid.* **80**, 2133 (1998).
[7] A. Ting *et al.*, Phys. Plasmas **4**, 1889 (1997).
[8] C. I. Moore *et al.*, Phys. Rev. Lett. **79**, 3909 (1997).
[9] P. Sprangle *et al.*, Phys. Rev. Lett. **69**, 2200 (1992); J. Krall *et al.*, Phys. Rev. E **48**, 2157 (1993).
[10] E. P. Lee and R. K. Cooper, Part. Accel. **7**, 83 (1976).
[11] P. Sprangle *et al.*, Phys. Rev. Lett. **79**, 1046 (1997).
[12] J. F. Reintjes, *Nonlinear Optical Parametric Processes in Liquids and Gases* (Academic, Orlando, FL, 1984).
[13] C. Max *et al.*, Phys. Rev. Lett. **33**, 209 (1974).
[14] E. S. Weibel, Phys. Rev. Lett. **2**, 83 (1959).
[15] R. C. Davidson, *Physics of Nonneutral Plasmas* (Addison-Wesley, Redwood City, CA, 1990).
[16] C. A. Kapetanakos, Appl. Phys. Lett. **25**, 484 (1974); R. B. Miller, *An Introduction to the Physics of Intense Charged Particle Beams* (Plenum Press, New York, 1982).
[17] A. D. Steiger and C. H. Woods, Phys. Rev. A **5**, 1467 (1972); Y. Horovitz *et al.*, Phys. Rev. Lett. **78**, 1707 (1997).
[18] T. Lehner, Phys. Scr. **49**, 704 (1994); Z. M. Sheng and J. Meyer-ter-Vehn, Phys. Rev. E **54**, 1833 (1996).
[19] K.-C. Tzeng *et al.*, Phys. Rev. Lett. **79**, 5258 (1997).
[20] R. D. Ruth *et al.*, Part. Accel. **17**, 171 (1985).
[21] S. V. Bulanov *et al.*, Phys. Rev. Lett. **74**, 710 (1995); P. Mora and T. M. Antonsen, Phys. Plasmas **4**, 217 (1997); J. R. Marques *et al.*, *ibid.* **5**, 1162 (1998); K. Krushelnick *et al.*, Phys. Rev. E **57**, 2475 (1998).
[22] G. Shvets and J. S. Wurtele, Phys. Rev. Lett. **73**, 3540 (1994); P. Sprangle *et al.*, *ibid.* **73**, 3544 (1994).